Carbon Capture Science & Technology 14 (2025) 100355

Contents lists available at ScienceDirect

Carbon Capture Science & Technology

journal homepage: www.elsevier.com/locate/ccst

Full Length Article

CO_2 electroreduction to C2 products on bimetallic silver copper melamine complexes

Munzir H. Suliman [a], Muhammad Usman [a,*], Husain Al Naji [b], Maryam Abdinejad [c], Naimat Ullah [a], Aasif Helal [a], Mahmoud M. Abdelnaby [a], Guillermo Díaz-Sainz [d], Gabriele Centi [e]

[a] Interdisciplinary Research Center for Hydrogen Technologies and Carbon Management (IRC-HTCM), King Fahd University of Petroleum & Minerals (KFUPM), Dhahran 31261, Saudi Arabia
[b] Research and Development Center, Saudi Aramco, Dhahran 31311 Saudi Arabia
[c] Department of Chemical Engineering, Delft University of Technology, 9 van der Maasweg, Delft 2629HZ, the Netherlands
[d] Departamento de Ingenierías Química y Biomolecular, Universidad de Cantabria, ETSIIT, Avda. Los Castros s/n 39005, Santander, Spain
[e] Department of ChiBioFarAm, University of Messina, v.le F. Stagno D'Alcontres 31, Messina 98166, Italy

ARTICLE INFO

Keywords:
Carbon conversion and utilization
Ag-cu melamine complex
Flow cell
Ethylene
Ethanol
Climate action
Affordable and clean energy

ABSTRACT

Nanocube crystals of bimetallic Ag-Cu-Melamine molecular complexes have been originally developed as effective electrocatalysts for the CO_2 selective reduction to multicarbon products, particularly ethylene and ethanol. The bimetallic complex, containing 10 wt.% Ag demonstrates the highest performance in electro-reduction of CO_2 in both H-type and flow cells. It achieves a Faradaic efficiency of 70 % for C2 products, with 40 % attributed to ethanol and the remaining to ethylene. These results are obtained at a cathode potential of -1.0 V vs reversible hydrogen electrode (RHE) with a total current density of -50 $mA{\cdot}cm^{-2}$ in the flow cell, five times higher current densities than the current densities in the H-Cell. Without Ag in the complex, only C1 products (CO and formic acid) are detected. The use of the flow cell, in addition to higher current densities, enhances C2 formation, especially ethylene, which is absent in H-type cell experiments. These novel electrocatalysts also exhibit stable performances and provide mechanistic indications of the roles of Ag and tandem cooperation with Cu.

Introduction

Developing efficient catalytic technologies based on renewable energy sources for carbon dioxide (CO_2) utilisation is a current target worldwide to create economic and environmentally sound alternatives to CO_2 storage, fostering a carbon circular and resilient economy (Centi and Perathoner, 2023; Khan et al., 2024; Quan et al., 2021; Tian et al., 2024; Usman, 2022). Electrocatalytic CO_2 conversion (CO_2RR) to multicarbon products is a significant challenge, serving as a core technology for synthesising raw materials for chemical production from CO_2 to substitute fossil fuels and move towards a carbon circular economy (Din et al., 2022; Jaster et al., 2022; Li et al., 2014; Papanikolaou et al., 2022; Usman et al., 2023). This area has garnered considerable research attention, and various recent reviews have also discussed the latest developments (Chang et al., 2023a; Hoque et al., 2024; Kuang and Zheng, 2023; Usman et al.).

Among the various catalysts investigated for CO_2RR to multicarbon products, those based on Cu-Ag allows are emerging as one of the more valuable options (Chen et al., 2020; Du et al., 2023; Suliman et al., 2024b). Cu is considered the element favouring C–C bond formation, while Ag enhances the first step of CO_2 conversion to CO (Amin et al., 2024; Li et al., 2019; Li et al., 2020). The surface coverage of CO on Cu is indicated as a key factor determining the C–C coupling (Chang et al., 2023b; Zhang et al., 2024a), and the role of Ag is to increase this coverage by promoting the CO_2 to CO reaction, eventually acting as a tandem co-catalyst (Wei et al., 2023). The electronic and geometric structure of bimetallic Ag–Cu alloys determine the selectivity (Israr et al., 2024; Zhang et al., 2020). On the other hand, Xue et al. (2023) indicate that the role of Ag modifies the electronic properties of Cu, creating oxygen defects on the catalyst surface, improving the adsorption and activation of CO_2 molecules. Frisch et al. (2023) indicate that bulk and surface lattice strain in Cu-Ag tandem catalysts determine the selectivity and the path to multicarbon products.

The use of Cu-Ag complexes as electrocatalysts has yet to be thoroughly investigated, even with various studies using copper molecular complexes for CO_2RR (Kim et al., 2022). Multimetallic Cu complexes promote C–C bond formation by coupling multiple bound $CO_2^{\bullet-}$ species but generate oxalic acid rather than products such as ethylene and ethanol (Li et al., 2021; Song et al., 2023; Su et al., 2023; Wang et al., 2024; Xu et al., 2024; Zhang et al., 2024b; Zhu et al., 2024). Molecular

* Corresponding author.
E-mail address: muhammadu@kfupm.edu.sa (M. Usman).

https://doi.org/10.1016/j.ccst.2024.100355
Received 7 November 2024; Received in revised form 28 November 2024; Accepted 21 December 2024

bicentric copper complexes are active in ethanol production by CO_2RR, but upon generation of small Cu clusters (Yang et al., 2022).

In conclusion, Cu-Ag bimetallic electrocatalysts have been studied for multicarbon CO_2RR but mainly as metallic alloys or tandem nanoparticles. The often indicated design strategy is to have either Ag and Cu separate nanoparticles (in tandem systems) or Ag- and Cu-rich zones (in the alloy), where the separate electrocatalytic steps of CO_2 to CO selective conversion (on Ag) and CO conversion to multicarbons (on Cu) cooperates via mediated transport of CO^* from the Ag to Cu sites (Chang et al., 2023a; Zhang et al., 2022). However, as commented above, other results contradict this design strategy for multicarbon CO_2RR catalysts. The study of bimetallic Cu-Ag molecular complexes as nanocrystalline electrocatalysts for CO_2RR could thus provide useful indications into these questions, besides offering new clues to prepare original electrocatalysts for this reaction. Cu and Ag ions are nearby but not present as alloy or metallic nanoparticles.

On the other hand, they can be used as molecular nanocrystals, thus offering a more homogeneous comparison with alloy and tandem-type Ag-Cu electrocatalysts. To our knowledge, molecular complexes were used as electrocatalysts only as isolated supported complexes rather than as molecular nanocrystals. This study may thus open new avenues in the design of electrocatalysts for multicarbon CO_2RR.

In addition, the coverage of CO_2 on the electrocatalyst has often been indicated as a key factor in determining multicarbon paths (Giusi et al., 2022). The use of a simple electrocatalytic cell design such as H-cell, in contrast to flow cells where the electrode design favours a higher surface CO_2 concentration on the electrocatalysts, has often led to large variations in the performances and selectivity to multicarbon products of the electrocatalysts (Ampelli et al., 2023). Therefore, a way to understand the role of surface coverage in determining the paths of transformation is to compare the performances of these two electrocatalytic cells. The results in flow cells, allowing significantly higher current densities, are also relevant from the application perspective.

In this context, the aim of this work is to investigate bimetallic silver copper melamine (Mel) complexes as electrocatalysts in the electrocatalytic reduction of CO_2 to C2 products (ethanol and ethylene) using both H-cell and flow cells. The results provide valuable indications on the role of these bimetallic complexes as novel molecular electrocatalysts and indications about the role and cooperation between Cu and Ag to generate active catalysts for this challenging reaction.

Experimental section

Synthesis of copper and silver-copper melamine complexes

A solution containing 170 mg of copper chloride dihydrate ($CuCl_2{\cdot}2H_2O$) was prepared by dissolving it in 20 ml of methanol purged with nitrogen gas. Subsequently, 250 mg of melamine was added to the solution. The solution underwent thermal treatment at 100 ˚C for 14 h. Afterward, the solution was cooled to room temperature, resulting in the collection of a green powder. This powder underwent three rounds of centrifugation with diethyl ether, followed by a final drying process under vacuum conditions at 50 ˚C.

The procedure for Ag-Cu melamine (Ag-Cu-Mel) complex formation in Fig. 1a was analogous, but silver nitrate was also added to the methanol solution. The weight ratios of silver to copper were 5 %, 10 %, and 20 %.

Electrode preparation

Ten mg of the catalyst was dispersed in a solution containing 750 µL of isopropanol, 200 µL of deionised water, and 50 µl of Nafion (5 %). The total volume was 1 mL. The solution was sonicated for 20 min. Following that, a suspension of 100 µl was applied to a conductive carbon paper with a surface area of 1 cm^2 using the drop-casting method. The sample was then allowed to dry at room temperature.

Electrochemical tests and experiments

CO_2RR behaviour was initially studied in an H-cell system (Fig. 1b) that includes a silver-silver chloride electrode (Ag/AgCl) as a reference electrode. A platinum mesh counter electrode was utilised. The working electrode was applied to a conductive carbon paper as the substrate. The electrodes in the cell are connected to a potentiostat, specifically the Gammray 620 model.

The CO_2RR performance was assessed by implementing linear sweep voltammetry (LSV) methodologies, involving determining the overpotential at various current densities, with the current values normalised to the geometric surface area of the electrode (1 cm^2). All potentials in this study were normalized to the RHE using the formula:

$$E_{RHE} = E_{Ag/AgCl} + 0.059 * pH + E^{\circ}_{Ag/AgCl}$$

Where $E^{\circ}_{Ag/AgCl} = 0.199\ V$

The Tafel slopes were estimated by using the equation:

$$= -A + log_{10}\frac{i}{io}$$

The Tafel region corresponds to the part of the function well approximated with the Tafel equation. In the Tafel equation, η is overpotential (V); i is current density (A/m^2); i_0 is exchange current density (A/m^2) when $\eta = 0$; A is Tafel slope.

A flow cell (Fig. 1c) was also used to verify the performances at higher current densities. The CO_2RR performances were evaluated at various potentials (−0.6 to −1.2 V vs. RHE) in tests of 1 h duration. Subsequently, the liquid products were extracted from the cell and quantified using H1-NMR. In contrast, the gaseous products were analysed by GC-BID, e.g. a gas-chromatograph with a barrier discharge ionisation detector, which allows two orders of magnitude higher sensitivity with respect to TCD detectors for gas phase components.

The cyclic voltammetry (CV) and linear sweep voltammetry (LSV) tests were carried out using a 0.5 M potassium bicarbonate ($KHCO_3$) solution. The voltage range was from 0.0 to −1.5 V versus RHE, e.g., the reversible hydrogen electrode.

$$Faradaic\ Efficiency\ (FE) = \frac{nZF}{Q} = \frac{nZF}{It} = \frac{nZF}{IV/v} * 100\ \%$$

n is the amount of product detected (number of moles, mol); Q is the total charge passed through the system, recorded during electrolysis (coulombs, C); F is the Faraday constant (96,485 C/mol); Z is the number of electrons required to obtain 1 molecule of the product; is the recorded current (A); t is the time required to fill the sampling loop (s); V is the volume of the sampling loop (cm^3); n is the recorded flow rate (ml/s).

The electrochemical impedance spectroscopy (EIS) was conducted by modulating the frequency range from 105 to 0.1 Hz while maintaining consistent electrolyte and electrode conditions as in the linear sweep voltammetry (LSV) experiment.

Results and discussion

Characterisation of the electrocatalysts

X-ray diffraction (XRD) was carried out to investigate the phase formation and purity of the prepared material. Fig. 2a demonstrates sharp reflection peaks between angles 10° and 30° for the Cu-Mel samples. The sharp peaks at low diffraction angles, with no appearance of Cu precursor and melamine peaks, indicate the formation of a complex.

An identical diffraction pattern to Cu-Mel was observed for the Ag-Cu-Mel sample, with an additional peak at 14° The intensity of this peak increased with the Ag content, confirming the formation of an Ag-Cu complex.

The EDX (Energy-dispersive X-ray spectroscopy) of the 10 % Ag-Cu-Mel shows the homogeneous presence of all elements (Cu, Ag, O, N, and Cl) without segregation. The ratio between Ag and Cu corresponds

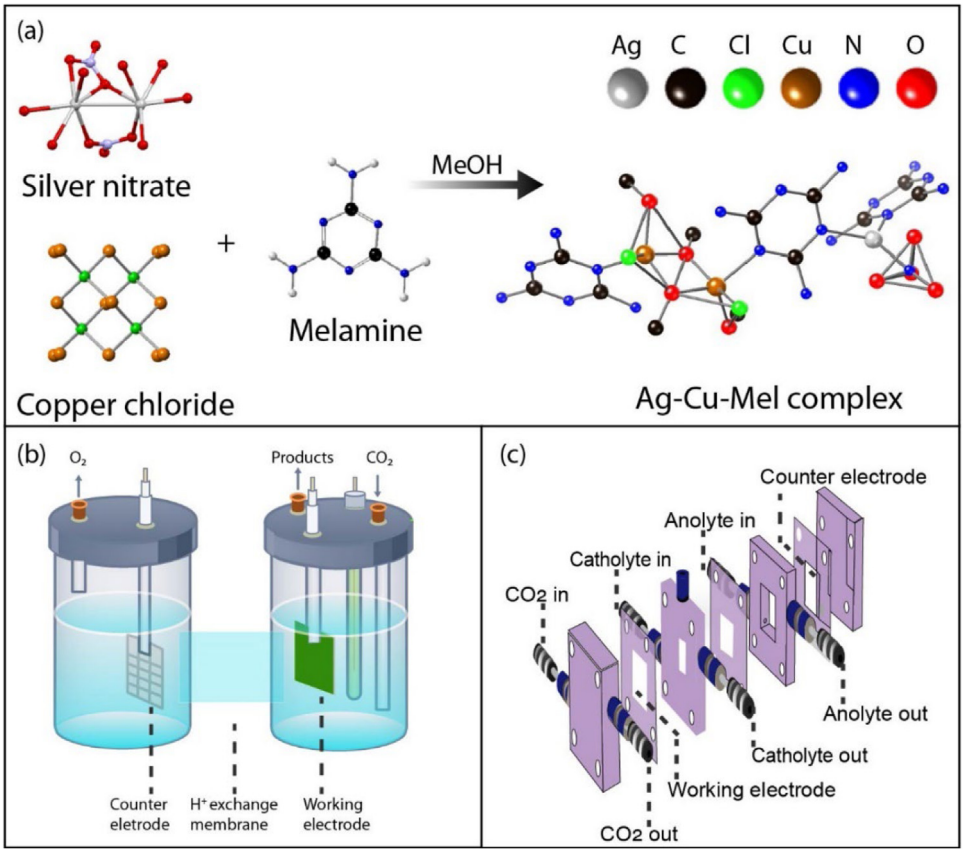

Fig. 1. Schematic illustration of (a) Ag-Cu-Mel complex formation, (b) H-cell configuration, and (c) flow cell configuration.

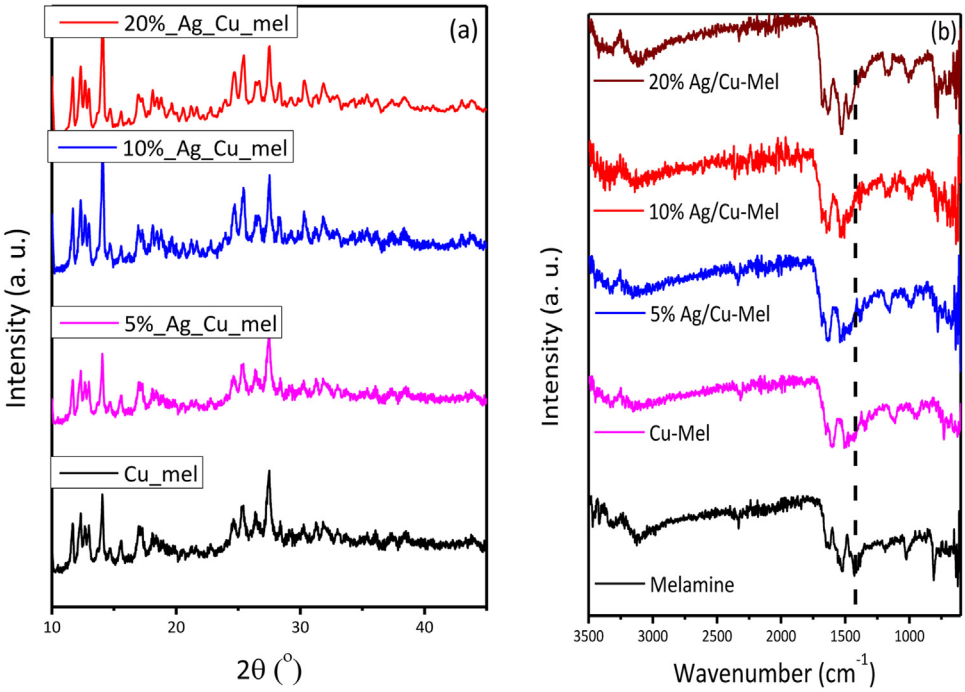

Fig. 2. (a) XRD and (b) The FT-IR of Cu-Mel, 5-Ag-Cu-Mel, 10 % Ag-Cu-Mel and 20 % Ag-Cu-Mel.

to what is expected based on the preparation ratio, additionally the elemental mapping confirms the homogenous dispersion of the elements in the sample (**Figure S1 & S2** in the *Supplementary Info*).

The FT-IR was performed for the complexing agent (melamine) and the four complexes. The peak for (-NH) bending vibration at 1460 cm^{-1} was blue shifted due to the metal binding with the triazine nitrogen in the melamine ring, in decanting the complexation of melamine (Vírseda et al., 2021; Wiles et al., 2006) (Fig. 2b).

The sample 10 % Ag-Cu-Mel was analysed using XPS (X-ray photoelectron Spectroscopy) (Fig. 3). The survey spectrum confirms the presence of all elements, e.g. C and N from melamine and Ag and Cu. The Cu, Ag, Cl, N, and C spectra agree with the expectations for the Ag-Cu-Mel

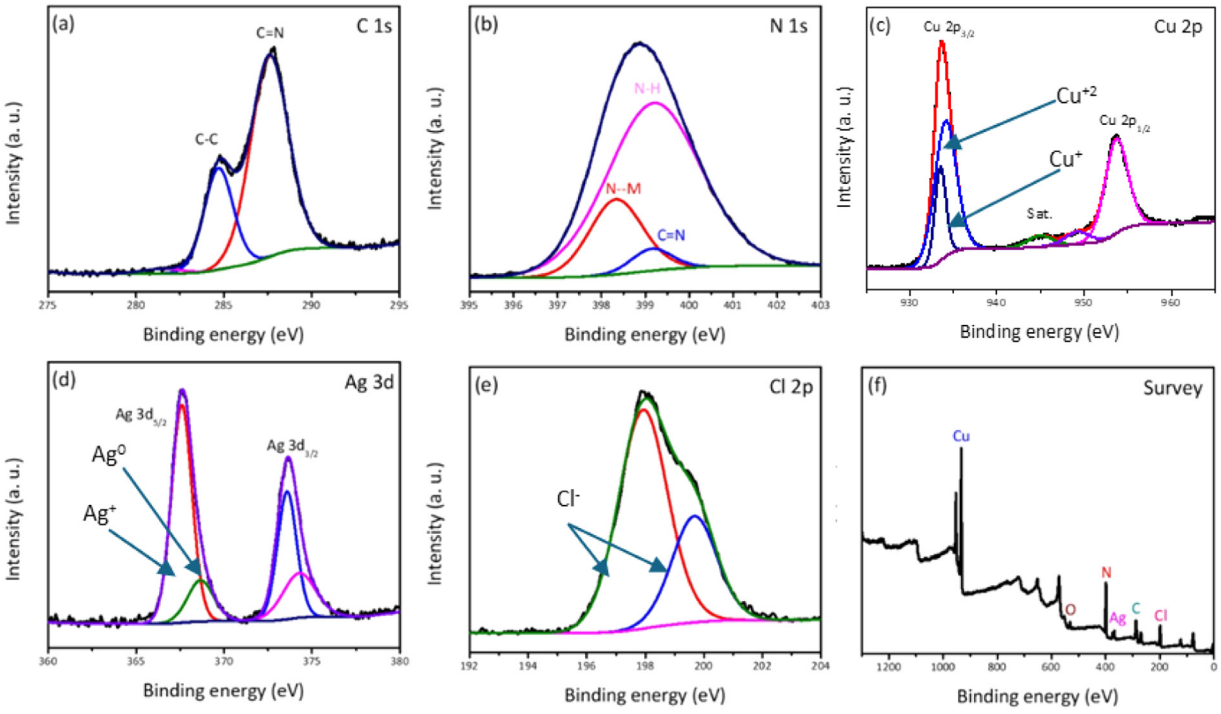

Fig. 3. XPS spectra of 10 % Ag-Cu-Mel in the (a) C 1 s, (b) N 1 s, (c) Cu 2p, (d) Ag 3d, (e) Cl 2p regions. The (f) image is the survey spectrum.

complex. The melamine showed in the C 1 s and N 1 s which is deconvoluted to several sub-peaks: the N–H, the triazene (C = N) and the coordinated N (Sun et al., 2022). The Cu 2p XPS spectrum of shows the spin-orbital doublets of $Cu2p_{1/2}$–$Cu2p_{3/2}$ lines for two oxidation states of copper: Cu^{+2} and Cu^{+1} at binding energies of 932.4 eV and 930.6 eV, respectively. From the Cu $2P_{3/2}$ spectrum the ratio between the Cu^{+} and Cu^{+2} was 30:70 %. The spectra of Ag, Cl and N confirms that the elements are part of the complex, additionally, **Table S1** shows the ratio of elements and Ag:Cu are with atomic ratio of 0.87: 13.7 which is around 10 wt% of Ag to Cu in the complex. According to the proposed structure of the complex the Ag is in the form of silver (I) (Vírseda et al., 2021; Wiles et al., 2006), which is in a good agreement with the XPS of Ag 3d spectrum (Ag^{+} is predominant around 81 atomic %). The Cl 2p spectrum is corresponidng to the inorganic chloride coming from the $CuCl_2$ in the complex (Han et al., 2014).

The scanning electron microscope (SEM) was used to investigate the morphological and structural features of the synthesised electrocatalysts (Fig. 4a). **Figure S3** displays the SEM images for Cu-Mel, 5 % Ag-Cu-Mel, 10 % Ag-Cu-Mel, and 20 % Ag-Cu-Mel. The sample exhibits distinct crystals with a semi-cubic form when observed using SEM. The TEM (Transmission Electron Microscopy) images (Fig. 4b) of the sample showed a similar morphology to that indicated by SEM images. High-resolution TEM (HRTEM) image (Fig. 4c) evidence that these nanocubes, of size around 30–50 nm, are well crystalline and have interlayer distance corresponding to copper-melamine complexes (Vírseda et al., 2021; Wiles et al., 2006). Selected area electron diffraction (SAED) measurements (Fig. 4d) confirm the indication.

Electrochemical characterisation and H-cell electrocatalytic tests

Linear sweep voltammetry (LSV) was used to characterise the electrochemical features of the electrodes. The polarisation curves for the electrodes Cu-Mel, 5 % Ag-Cu-Mel, 10 % Ag-Cu-Mel, and 20 % Ag-Cu-Mel are shown in Fig. 5a. Tests were carried out in an electrolyte saturated with CO_2. The current density in Cu-Mel, without Ag, is significantly lower. The loading with 5 % Ag resulted in a considerable rise in the current density, from 8 to 16 $mA{\cdot}cm^{-2}$. The current density increased with the amount of Ag loading, reaching a maximum of 35 $mA{\cdot}cm^{-2}$ for 5 % Ag-Cu-Mel and a value of 27 $mA{\cdot}cm^{-2}$ for 10 % Ag loading.

Tafel slope values (Fig. 5b) confirm that the 10 % Ag-Cu-Mel possesses the fastest kinetics. Electrochemical impedance spectroscopy (EIS) was employed (Fig. 5c) to study the kinetics of electrochemical processes further. It provides indications of the resistances dominating the processes at the interface between the electrode and electrolyte. The charge transfer resistance (R_{ct}) was determined from the Nyquist plot (Hallemans et al., 2023; Macdonald, 1990; Randviir and Banks, 2022; Suliman et al., 2022; Suliman et al., 2024a). The reported values for the R_{ct} were 10, 19, 30, and 45 Ω cm^2 for the electrodes with compositions of 20 % Ag-Cu-Mel, 10 % Ag-Cu-Mel, 5 % Ag-Cu-Mel, and Cu-Mel, respectively. The results prove that adding Ag to Cu-Mel greatly enhances the charge transfer rate. The 20 % loading exhibits the lowest R_{ct} among the different samples investigated. The partial current density in 0.5 M $KHCO_3$ electrolyte shows a maximum for an applied potential of −1.0 V vs RHE (V_{RHE}), as shown in Fig. 5d for 10 %Ag-Cu-Mel. The decrease in current density above this value is due to an increased hydrogen evolution reaction, as seen below.

The Faradaic Efficiency (FE) of the electrodes was determined by running chronoamperometry experiments for 60 min in the H-cell (Fig. 6), online connected to the GC-BID to investigate the gaseous products. The liquid sample was collected at the end to determine the liquid products using 1H–NMR (water suppression method). In Cu-Mel (Fig. 6a), three products were observed: H_2, CO, and HCOOH. The HCOOH ratio increased with the potential to reach FE of 57 % at 1.0 V_{RHE}; after that, it decreased due to an increase in the H_2 ratio derived from HER (hydrogen evolution reaction). After introducing a small amount of Ag in 5 %Ag-Cu-Mel (Fig. 6b), the trend was analogous. However, the FE_{CO} and FE_{HCOOH} increased, reaching a total FE in carbon products (CO + HCOOH) of over 95 % at 1.0 V_{RHE}. Ethanol started appearing as a liquid product in 10 % Ag-Cu-Mel (Fig. 6c) with a ratio of 40 % at a potential of 1.0 V_{RHE}. In 20 % Ag-Cu-Mel (Fig. 6d), the ethanol FE decreases at the expense of a higher FE_{CO}.

The electrode durability was investigated using chronoamperometry (**Figure S4**) in 0.5 M $KHCO_3$. The long-term current time curve revealed

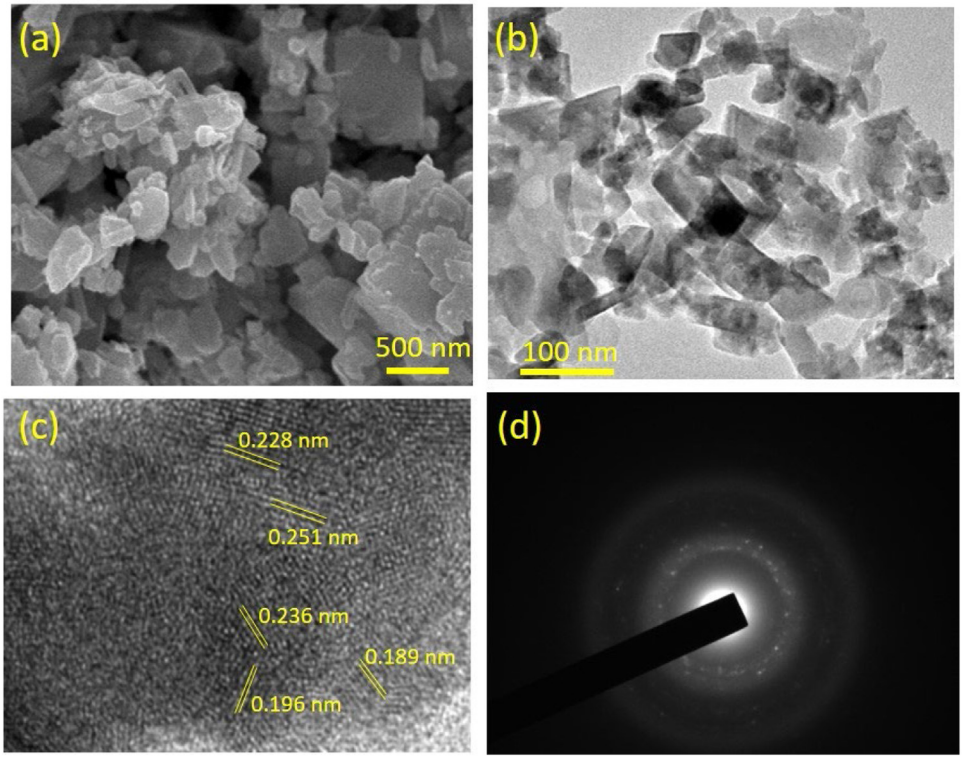

Fig. 4. (a) SEM image of 10 %Ag-Cu-Mel; (b) TEM and (c) HRTEM images; (d) SAED (Selected area electron diffraction).

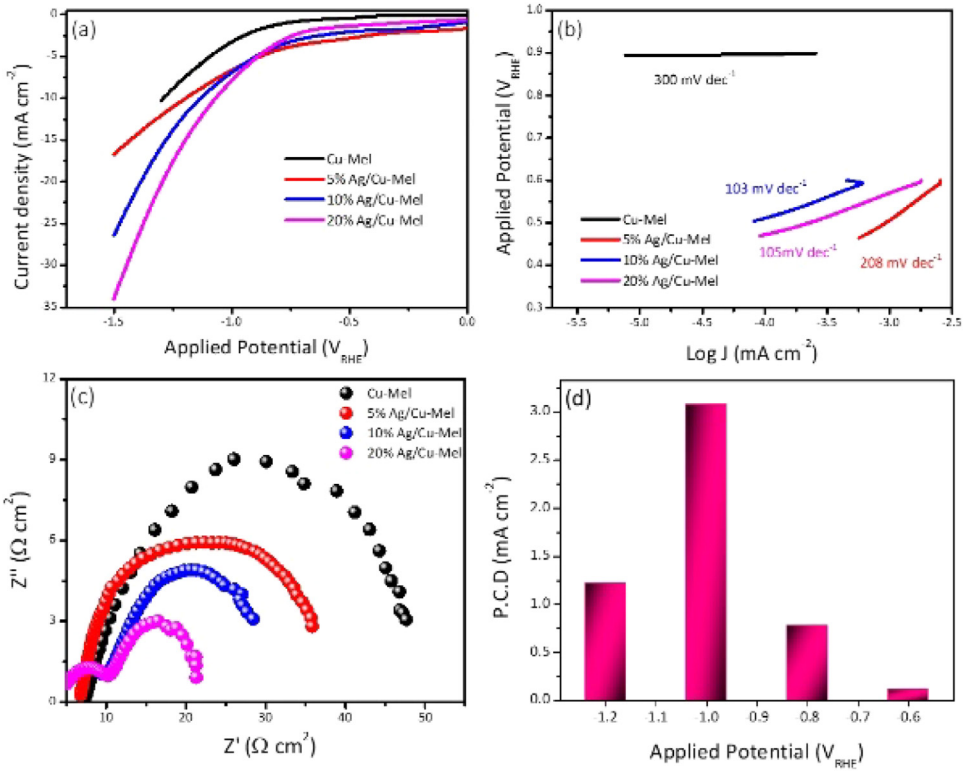

Fig. 5. (a) LSV, (b) Tafel slopes and (c) EIS of Cu-Mel, 5 %Ag-Cu-Mel, 10 %Ag-Cu-Mel and 20 % Ag-Cu-Mel (d) the partial current density of 10 %Ag-Cu-Mel in 0.5 M $KHCO_3$ electrolyte).

good stability for 12 h with no significant loss in the current or the product formation.

Electrocatalytic performances in flow cell

In addition to the tests in the H–Cell, the optimal electrode (10 % Ag-Cu-Mel) was also investigated in the flow cell. As commented in the introduction and more extensively elsewhere (Suliman et al., 2024b; Usman and Suliman, 2023; Xu et al., 2024), the use of gas-diffusion electrodes (GDL) allows for enhancement of the surface coverage of CO_2 on the electrocatalysts. These electrodes are in direct contact with gas-phase CO_2, rather than being limited by CO_2 solubility. From a practical perspective, these cells and electrodes allow significantly higher current densities, making them crucial from applications. On the other hand, the

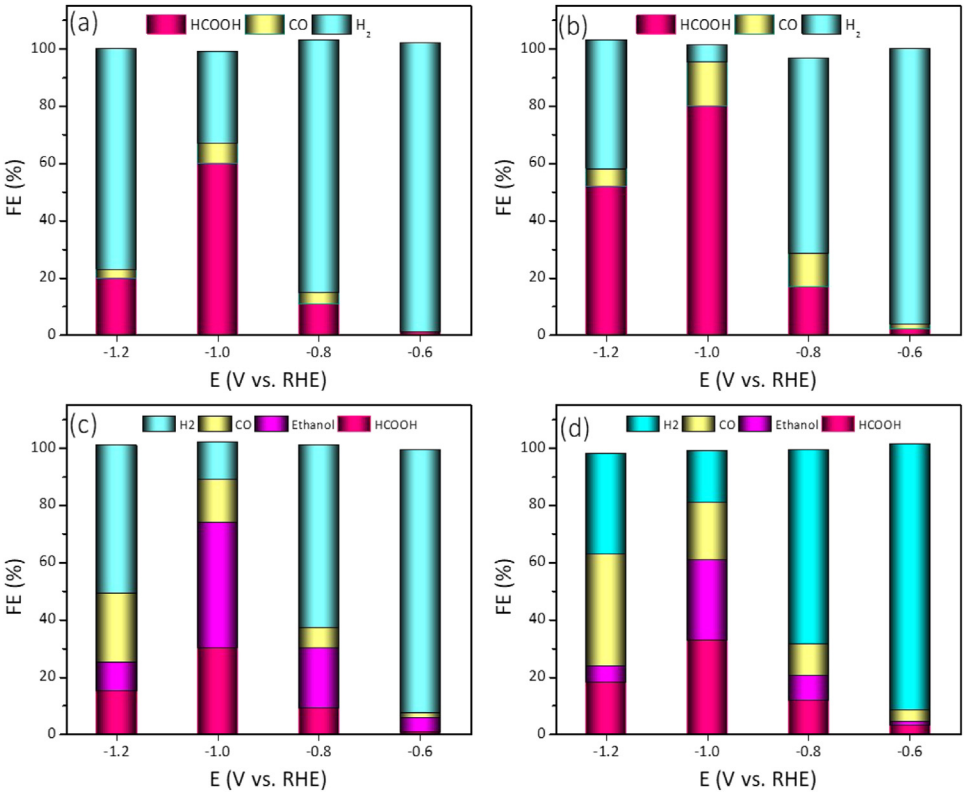

Fig. 6. FE (in H-cell tests) of (a) Cu-Mel, (b) 5 %Ag-Cu-Mel, (c) 10 %Ag-Cu-Mel and (d) 20 % Ag-Cu-Mel.

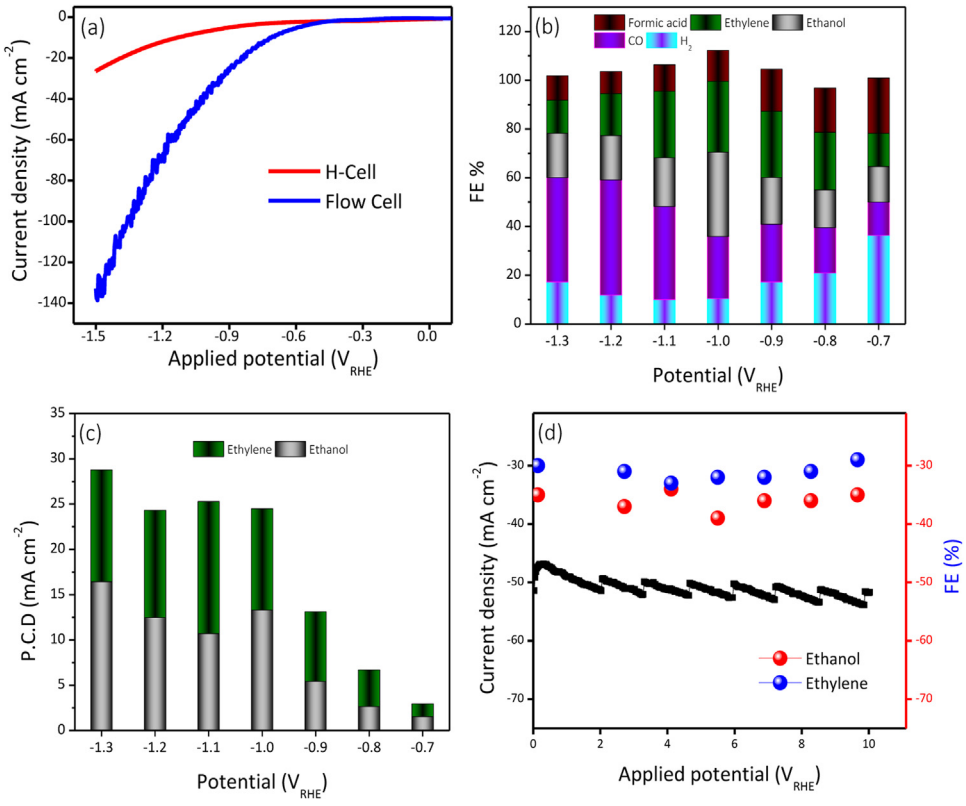

Fig. 7. (a) Comparative LSV of the H-cell and the flow cell. Tests in flow cell: (b) FE, (c) partial current density and (d) stability of 10 % Ag-Cu-Mel.

comparison between the results in H-cell and flow cell provides indications on whether the surface coverage of CO_2 (or CO deriving from it) is crucial in determining the selectivity to multicarbon products in CO_2RR, as indicated as a role of Ag (see introduction).The LSV and FE values obtained from the flow cell were compared to those obtained in H–Cell for the same electrocatalyst (10 % Ag-Cu-Mel) (Fig. 7a). The experimental setup and schemes of the H-cell and flow cell are shown in Figs. 7c and 7d, respectively. Different surface concentrations of COx species also change the dependence of FE on the applied voltage (Fig. 7b). In addition, the formation of ethylene together with ethanol is also detected. The best performances as FE are also shown at a −1.0 V_{RHE}. The total FE to carbon products (excluding H_2) is around 90 %, although there

are some ±10 % errors in estimations of the total FE due to analytical methods. Apart from about 12 % FE_{HCOOH} and 25 % FE_{CO}, ethylene and ethanol are the main products of CO_2RR, with FEs of 29 % and 38 %, respectively. These are good performances with respect to literature, considering that the systems are not optimised and that very good current densities are obtained simultaneously (Fig. 6c), e.g. 50 mA·cm^{-2} at −1.0 V_{RHE}.

The current density in the flow cell is significantly higher than in the H-cell (Fig. 7a) due to the Gas Diffusion Electrode (GDE), which enhances the diffusion of CO_2 onto the catalyst's surface. Furthermore, the flow system provides a continual supply of fresh electrolytes to the surface of the electrodes, increasing the overall efficiency of the reaction. A 180 mA·cm^{-2} current density was attained at 1.5 V_{RHE}, more than ten times greater than the current recorded in the H–Cell. As shown in Fig. 6b, increasing the concentration of CO_2 at the catalyst surface increases the reduction reaction, resulting in high current density and enhanced CO_2 conversion rates. It is worth mentioning that the hydrogen evolution process (HER) was significantly suppressed as compared to the H–Cell. FE_{H2} was a minimum in the negative 1.1–1.0 V_{RHE} range. A single liquid product, formic acid, was identified with faradaic efficiencies ranging from 10 % to 25 %. carbon monoxide (CO) concentration increased and reached an FE of 55 % at 1.2 V compared to the RHE. At high potentials, the concentration of CO remained relatively stable. A similar pattern was observed in the case of ethylene, which reaches a maximum FE of 32 %. $FE_{Ethanol}$ was 38 % at the best. The partial current density for ethanol in the flow cell was 10 mA·cm^{-2} (Fig. 6c), which was much higher than that in the H–Cell (about 3.0 mA·cm^{-2}). Fig. 6d shows the long-term stability of 10 %Ag-Cu-Mel in flow cell for 10 h showing a continuous production of ethanol and ethylene at high current density of 50 mA/cm^2. Moreover, the XRD diffraction of the complex was investigated before and after the electrolysis and there was no significant change in complex diffraction after the stability test as shown in figure S6.

Cu-Ag-Mel as efficient catalysis in multicarbon CO_2RR

The 10 % Ag-Cu-Mel complex exhibits valuable performances in multicarbon CO_2RR, achieving an optimal $FE_{ethanol+ethylene}$ of over 70 % at relevant current densities (50 mA·cm^{-2} at −1.0 V_{RHE}) in a flow cell. Further optimisation and performance enhancement are possible by tuning the size of the Ag-Cu-Mel molecular complex nanocubes and optimising the Ag content. The results are well comparable with those reported in the literature, suggesting that nanocrystalline Ag-Cu-Mel molecular complex provide performances analogous to those of Ag-Cu alloys or tandem systems. **Table S2** reports a comparison with selected literature results.

To our knowledge, this is the first time demonstration of Ag-Cu molecular complexes exhibiting good performances in multicarbon CO_2RR. Moreover, they have been used as molecular nanocrystals rather than isolated complexes supported on a conductive material. This suggests new possibilities for designing original electrocatalysts with stable performances. While our tests on Ag-Cu-Mel complex nanocrystals demonstrate stable behaviour, more extensive results would be necessary.

Although AgCu single-atom (SAC) electrocatalysts have recently been reported [4a] to show better performances with a total FE to multicarbon products of over 90 % (including isopropanol and acetic acid) at a current density up to about 700 mA·cm^{-2} in a flow cell, our results confirm that Ag-Cu bimetallic complex, similar to $AgCu_{SAC}$, offer a valuable route, simpler and less costly from the preparation perspective to achieve high performances in the challenging CO_2RR to ethylene and ethanol. Compared to the state of the art, these results indicate that crystalline molecular Ag-Cu bimetallic complexes are a promising direction to explore for preparing electrocatalysts with enhanced properties.

Mechanistic implications for multicarbon CO_2RR

Our results do not support the idea of a tandem cooperation of Ag and Cu in these catalysts, as suggested by Du et al. (2023) and various other authors, for synthesising multicarbons in CO_2RR. This tandem concept assumes that CO_2 to CO conversion occurs on Ag sites physically separated from Cu sites, with CO* then transported from Ag to Cu sites. We have proven that, in our electrocatalysts, the Cu-Mel complex is inactive towards C2 products in CO_2RR, although it exhibits reasonably good behaviour towards C1 products (CO and formic acid). The formation of the Ag-Cu bimetallic complex leads to the enhanced selectivity of C2. However, only ethanol is formed in the H-cell, with ethylene formation occurring only when the flow cell is used. Thus, the increased coverage by CO_2 of the electrocatalysts, being in direct contact with gas CO_2 rather than with CO_2 dissolved in the electrolyte, changes the selective conversion pathways, in addition to allowing significantly higher CO_2 conversion (current density).

On the other hand, the copper and silver atoms are co-present in the bimetallic Ag-Cu molecular complex. Thus, there is a synergic cooperation and an electronic effect between Ag and Cu atoms rather than a tandem mechanism. However, the effect of the coverage of CO_x on the product distribution, when changing from H-type to flow cell, indicates that both Ag and Cu atoms in the bimetallic complex should coordinate CO_x species to enable the multicarbon path. Vicinal multimetallic sites determine the possibility of forming C2 products selectively rather than using a tandem mechanism. This solution also reduces the side HER reaction. The overall carbon FE in CO_2RR, with respect to side H_2 evolution reaction, reaches over 90 % in the best conditions, demonstrating a valuable performance. The better overall carbon FE in CO_2RR using flow cell rather than an H-cell confirms the role of CO_x chemisorption in controlling this side reaction.

Conclusion

A bimetallic Ag-Cu-Melamine molecular complex, used as small nanocube-type crystals, shows valuable performances in multicarbon CO_2RR, particularly when utilized in flow cells. The FE to ethylene and ethanol reaches 70 % with an overall carbon FE of 90 % in 10 % Ag-Cu-Mel at −1.0 V_{RHE}. This marks the first instance of these molecular complexes demonstrating such high and stable performances in multicarbon CO_2RR, showcasing the potential use of molecular nanocrystals as novel electrocatalysts.

The results also provide mechanistic insghts into the roles of Ag and Cu and whether tandem mechanisms with CO* intermediate channelled from Ag to Cu sites are necessary to obtain high performances in ethanol and ethylene. Additionally, the study highlights how the flow cell, aside from higher current densities, promotes enhanced C2 formation, especially ethylene, in which is absent in H-type cell experiments. Thus, the cell configuration influences productivity and affects the type and distribution of the formed products.

Declaration of competing interest

The authors declare that they have no known competing financial interests or personal relationships that could have appeared to influence the work reported in this paper.

CRediT authorship contribution statement

Munzir H. Suliman: Writing – original draft, Software, Methodology, Investigation, Formal analysis, Data curation, Conceptualization. **Muhammad Usman:** Writing – review & editing, Writing – original draft, Visualization, Validation, Supervision, Resources, Data curation, Conceptualization. **Husain Al Naji:** Validation, Software, Methodology, Data curation. **Maryam Abdinejad:** Writing – review & editing, Visualization, Software, Investigation. **Naimat Ullah:** Visualization, Valida-

tion, Supervision, Resources. **Aasif Helal:** Methodology, Formal analysis, Conceptualization. **Mahmoud M. Abdelnaby:** Validation, Software, Investigation, Data curation. **Guillermo Díaz-Sainz:** Visualization, Validation, Investigation, Data curation. **Gabriele Centi:** Visualization, Validation, Investigation, Conceptualization.

Acknowledgements

The author would like to acknowledge the support provided by King Fahd University of Petroleum & Minerals (KFUPM) and the support from Saudi Aramco Chair Professor Program at KFUPM No ORCP2390.

Funding

This work was supported by KFUPM and Saudi Aramco Chair Professor program at KFUPM [grant number ORCP2390].

Supplementary materials

Supplementary material associated with this article can be found, in the online version, at doi:10.1016/j.ccst.2024.100355.

References

Amin, M., Usman, M., Kella, T., Khan, W.U., Khan, I.A., Hoon lee, K., 2024. Issues and challenges of Fischer–Tropsch synthesis catalysts. Front. Chem. 12, 1462503.
Ampelli, C., Tavella, F., Giusi, D., Ronsisvalle, A.M., Perathoner, S., Centi, G., 2023. Electrode and cell design for CO_2 reduction: a viewpoint. Catal. Today 421, 114217.
Centi, G., Perathoner, S., 2023. The chemical engineering aspects of CO_2 capture, combined with its utilisation. Curr. Opin. Chem. Eng. 39, 100879.
Chang, B., Pang, H., Raziq, F., Wang, S., Huang, K.W., Ye, J., Zhang, H., 2023a. Electrochemical reduction of carbon dioxide to multicarbon (C 2+) products: challenges and perspectives. Energy Environ. Sci..
Chang, X., Xiong, H., Lu, Q., Xu, B., 2023b. Mechanistic implications of low CO coverage on Cu in the electrochemical CO and CO_2 reduction reactions. JACS. Au 3, 2948–2963.
Chen, C., Li, Y., Yu, S., Louisia, S., Jin, J., Li, M., Ross, M.B., Yang, P., 2020. Cu-Ag tandem catalysts for high-rate CO_2 electrolysis toward multicarbons. Joule 4, 1688–1699.
Din, I.U., Nasir, Q., Garba, M.D., Alharthi, A.I., AlotaibI, M.A., Usman, M., 2022. A review of preparation methods for heterogeneous catalysts. Mini. Rev. Org. Chem. 19, 92–110.
Du, C., Mills, J.P., Yohannes, A.G., Wei, W., Wang, L., Lu, S., Lian, J.X., Wang, M., Guo, T., Wang, X., 2023. Cascade electrocatalysis via AgCu single-atom alloy and Ag nanoparticles in CO_2 electroreduction toward multicarbon products. Nat. Commun. 14, 6142.
Frisch, M.L., Wu, L., Atlan, C., Ren, Z., Han, M., Tucoulou, R., Liang, L., Lu, J., Guo, A., Nong, H.N., 2023. Unraveling the synergistic effects of Cu-Ag tandem catalysts during electrochemical CO_2 reduction using nanofocused X-ray probes. Nat. Commun. 14, 7833.
Giusi, D., MicelI, M., Genovese, C., Centi, G., Perathoner, S., Ampelli, C., 2022. In situ electrochemical characterization of CuxO-based gas-diffusion electrodes (GDEs) for CO_2 electrocatalytic reduction in presence and absence of liquid electrolyte and relationship with C2+ products formation. Appl. Cataly. B 318, 121845.
Hallemans, N., Howey, D., Battistel, A., Saniee, N.F., Scarpioni, F., Wouters, B., La mantia, F., Hubin, A., Widanage, W.D., Lataire, J., 2023. Electrochemical impedance spectroscopy beyond linearity and stationarity—A critical review. Electrochim. Acta, 142939.
Han, C., Ge, L., Chen, C., Li, Y., Zhao, Z., Xiao, X., Li, Z., Zhang, J., 2014. Site-selected synthesis of novel Ag@ AgCl nanoframes with efficient visible light induced photocatalytic activity. J. Mater. Chem. A 2, 12594–12600.
Hoque, B., Khan, M.Y., Hanif, A., Abdelnaby, M., Helal, A., Khan, A., Usman, M., Drmosh, Q.A., 2024. Tailored design of CO_2-selective mixed-matrix membranes using nitrile-functionalized COFs as 2D nanofillers. J. Environ. Chem. Eng. 12, 112695.
Israr, M., Humayun, M., Suliman, M.H., Abdinejad, M., Rasheed, T., Helal, A., Khan, I., Bououdina, M., Wang, C., Usman, M., 2024. Multi-metallic electrocatalysts as emerging class of materials: opportunities and challenges in the synthesis, characterization, and applications. Cataly. Rev. 1–61.
Jaster, T., Gawel, A., Siegmund, D., Holzmann, J., Lohmann, H., Klemm, E., APFEL, U.P., 2022. Electrochemical CO_2 reduction toward multicarbon alcohols-the microscopic world of catalysts & process conditions. Iscience, p. 25.
Khan, S., Khulief, Y., Juanes, R., BashmaL, S., Usman, M., Al-Shuhail, A., 2024. Geomechanical modeling of CO_2 sequestration: a review focused on CO_2 injection and monitoring. J. Environ. Chem. Eng., 112847.
Kim, K., Wagner, P., Wagner, K., Mozer, A.J., 2022. Electrochemical CO_2 reduction catalyzed by copper molecular complexes: the influence of ligand structure. Energy. Fuels 36, 4653–4676.
Kuang, M., Zheng, G., 2023. Interfacial microenvironments for carbon dioxide electro-upgrading to multicarbon products. Chem. Catal. 3.
Li, D., Zhang, H., Usman, M., Li, Z., Han, L., Li, C., Zhang, S., 2014. Study on the hydrotreatment of C9 aromatics over supported multi-metal catalysts on γ-Al_2O_3. J. Renew. Sustain. Energy 6.
Li, D., Zhang, H., Xiang, H., Rasul, S., Fontmorin, J.M., Izadi, P., Roldan, A., TayloR, R., Feng, Y., Banerji, L., 2021. How to go beyond C 1 products with electrochemical reduction of CO_2. Sustain. Energy Fuels. 5, 5893–5914.
Li, F., Li, Y.C., Wang, Z., Li, J., Nam, D.H., Lum, Y., Luo, M., Wang, X., Ozden, A., Hung, S.F., 2020. Cooperative CO_2-to-ethanol conversion via enriched intermediates at molecule–metal catalyst interfaces. Nat. Catal. 3, 75–82.
Li, J., Wang, Z., Mccallum, C., Xu, Y., Li, F., Wang, Y., Gabardo, C.M., Dinh, C.T., Zhuang, T.T., Wang, L., 2019. Constraining CO coverage on copper promotes high–efficiency ethylene electroproduction. Nat. Catal. 2, 1124–1131.
Macdonald, D.D., 1990. Review of mechanistic analysis by electrochemical impedance spectroscopy. Electrochim. Acta 35, 1509–1525.
Papanikolaou, G., Centi, G., Perathoner, S., Lanzafame, P., 2022. Catalysis for e-chemistry: need and gaps for a future de-fossilized chemical production, with focus on the role of complex (direct) syntheses by electrocatalysis. ACS. Catal. 12, 2861–2876.
Quan, Y., Zhu, J., Zheng, G., 2021. Electrocatalytic reactions for converting CO_2 to value-added products. Small. Sci. 1, 2100043.
Randviir, E.P., Banks, C.E., 2022. A review of electrochemical impedance spectroscopy for bioanalytical sensors. Analytic. Methods 14, 4602–4624.
Song, Z., Wang, X., Ren, Z., Fu, H., 2023. Relationships between structural design and synthesis engineering of Cu-based catalysts for CO_2 to C2 electroreduction. Chem. Eng. J., 147606.
Su, W., Guo, W., Fan, Y., 2023. CuAg bimetallic catalysts derived from an Ag-anchored Cu-based metal–organic framework for CO_2 electroreduction to ethanol. Chem. Eng. J. 477, 147204.
Suliman, M., Alarfaj, F., Usman, M., Alaqad, K.M., Hussein, M.A., Abdelnaby, M.M., 2024a. Boosting the electrocatalytic water splitting performance using hydrophilic metal-organic framework. Chem.–An Asian J., e202301129.
Suliman, M.H., Al naji, H., Usman, M., 2024b. Zn-Cu bimetallic gas diffusion electrodes for electrochemical reduction of CO2 to ethylene. Electrochim. Acta 500, 144723.
Suliman, M.H., Yamani, Z.H., Usman, M., 2022. Electrochemical reduction of CO_2 to C1 and C2 liquid products on copper-decorated nitrogen-doped carbon nanosheets. Nanomaterials 13, 47.
Sun, Y., Jing, H., Wu, Z., Yu, J., Gao, H., Zhang, Y., He, G., Lei, W., Hao, Q., 2022. High efficient catalyst of N-doped carbon modified copper containing rich Cu– N– C active sites for electrocatalytic CO_2 reduction. ChemistrySelect. 7, e202200557.
Tian, H., Zhang, Z.Y., Fang, H., Jiao, H., Gao, T.T., Yang, J.T., Bian, L., Wang, Z.L., 2024. Selective electrooxidation of methane to formic acid by atomically dispersed CuOx and its induced Lewis acid sites on V2O5 in a tubular electrode. Environ. Energy 351, 124001.
Usman, M., 2022. Recent progress of SAPO-34 zeolite membranes for CO_2 separation: a review. Membranes. 12, 507.
Usman, M., Al-Ghourani, A. & AL-Maythalony, B. Covalent Functionalization of Zif-90 for Improved CO2 separation by mixed matrix membrane. Available at SSRN *4136344*.
Usman, M., Garba, M.D., Zeb, Z., Israr, M., Safia, S., Javed, F., Suliman, M.S., Alfaify, B., Sanhoob, M.A., Iqbal, N., 2023. Co_2 conversion via catalytic hydrogenation to methanol, DME and Syngas. Springer Sustainable Utilization of Carbon Dioxide: From Waste to Product.
Usman, M., Suliman, M.H., 2023. Silver-Doped zeolitic imidazolate framework (Ag@ ZIF-8): an efficient electrocatalyst for CO_2 conversion to syngas. Catalysts. 13, 867.
Vírseda, I.B., Siddiqui, S.A., Prado-Roller, A., Eisterer, M., Shiozawa, H., 2021. Crystal engineering with copper and melamine. RSC Adv., 11, 23943–23947.
Wang, Y., Cheng, Q., Zhang, H., Ma, L., Yang, H., 2024. Cobalt (II) tetraphenylporphyrin trapped in the pores of Cu_2O to enhance the C2+ selectivity towards acidic CO_2 electroreduction. Chem. Eng. J. 492, 152254.
Wei, C., Yang, Y., Ma, H., Sun, G., Wang, X., Cheng, Y., Zhang, C., Yeo, B.S., HE, C., Wong, A.B., 2023. Nanoscale management of CO transport in CO_2 electroreduction: boosting faradaic efficiency to multicarbon products via nanostructured tandem electrocatalysts. Adv. Funct. Mater. 33, 2214992.
Wiles, A.B., Bozzuto, D., Cahill, C.L., Pike, R.D., 2006. Copper (I) and (II) complexes of melamine. Polyhedron. 25, 776–782.
Xu, Z., Zhang, X., Wang, Q., 2024. Tailoring the catalytic microenvironment of CuO with hydrophobic $CuSA_2$ for selective CO2 electroreduction to C2+ products. Chem. Eng. J. 492, 152164.
Xue, L., Fan, Q.Y., Zhao, Y., Liu, Y., Zhang, H., Sun, M., Wang, Y., Zeng, S., 2023. Ultralow Ag-assisted carbon–carbon coupling mechanism on Cu-based catalysts for electrocatalytic CO_2 reduction. J. Energy Chem. 82, 414–422.
Yang, B., Chen, L., Xue, S., Sun, H., Feng, K., Chen, Y., Zhang, X., Xiao, L., Qin, Y., Zhong, J., 2022. Electrocatalytic CO_2 reduction to alcohols by modulating the molecular geometry and Cu coordination in bicentric copper complexes. Nat. Commun. 13, 5122.
Zhang, B., Wang, L., Li, D., Li, Z., Bu, R., Lu, Y., 2022. Tandem strategy for electrochemical CO_2 reduction reaction. Chem. Catal. 2, 3395–3429.
Zhang, W., Xu, C., Hu, Y., Yang, S., Ma, L., Wang, L., Zhao, P., Wang, C., Ma, J., Jin, Z., 2020. Electronic and geometric structure engineering of bicontinuous porous Ag–Cu nanoarchitectures for realizing selectivity-tunable electrochemical CO_2 reduction. Nano Energy 73, 104796.
Zhang, Z.Y., Tian, H., Jiao, H., Wang, X., Bian, L., Liu, Y., Khaorapapong, N., Yamauchi, Y., Wang, Z.L., 2024a. SiO_2 assisted Cu 0–Cu+–NH_2 composite interfaces for efficient CO_2 electroreduction to C 2+ products. J. Mater. Chem. A 12, 1218–1232.
Zhang, Z., Wang, X., Tian, H., Jiao, H., Tian, N., Bian, L., Liu, Y., Wang, Z.L., 2024b. Highly dispersed Cu-Cu_2O-CeOx interfaces on reduced graphene oxide for CO_2 electroreduction to C2+ products. J. Colloid. Interface Sci. 661, 966–976.
Zhu, C., Wu, G., Mao, J., Chen, A., Zhao, Y., Feng, G., Wei, Y., Liu, X., Li, S., Li, G., 2024. Halide-modulated Hollow-Fiber Cu penetration electrode boosts Ampere-Level CO_2 electroreduction to multicarbon products. Chem. Eng. J. 485, 150040.